Notes on Host Galaxy Dust

E. D. Commins January, 2002

1. Basic facts about dust in our Galaxy.

Interstellar dust is an important constituent of our Galaxy, and of other galaxies as well. Galactic dust is mainly confined to the Galactic plane, and its total mass is roughly 1% of the mass of interstellar gas. It consists of sub-micron sized particles, mainly graphite (and/or other forms of carbon such as nanotubes, bucky-balls, etc.), silicates, polycyclic aromatic hydrocarbons (PAHs), and some ices (NH_3, H_2O). Dust plays an important role in the energy balance of the Galaxy because it absorbs starlight (mainly in the UV and visible) and re-radiates it in the far infra-red (FIR). Perhaps 30% of the total luminosity of the Galaxy is due to this re-radiation. The opacity of dust is generally a decreasing function of wavelength; thus dust causes reddening of transmitted starlight. Dust-induced extinction (from our Galaxy, but more importantly in a host galaxy, and possibly in intergalactic space) could be a significant source of systematic error in observations of supernovae.

Dust grains (and in particular, carbon particles) are probably formed in the outer envelopes of red giant stars and/or horizontal branch stars. A typical grain is exposed to many physical processes and undergoes radical transformations during its lifetime [Salpeter 1977]. Grain-grain collisions can cause grains to be shattered, but on the other hand in such collisions, grains can stick together to form larger objects (which in some cases can ultimately become asteroids and planets). Intense stellar radiation can evaporate volatile molecules from grain surfaces. UV can photo-ionize grains. Collisions with fast ions can sputter the grains (drive atoms from the grain surface). Shock waves from supernova remnants can fragment grains, and radiation pressure as well as gas-grain collisions can accelerate them. If grains are electrically charged, and undoubtedly a fraction are, then their motion is influenced by Galactic magnetic fields. All in all, a typical grain is influenced by many forces, and has a very complex history.

The absorption and reddening, which vary from one line of sight to another, are characterized by the following quantities, defined separately for each species of dust grain (as categorized by composition, size, and shape):

•The opacity per gram of the ith component $\kappa_\iota(\lambda)$ in cm^2/g (1)

• The mass density of the i'th dust component: ρ_i in g/cm^3 (2)

From these quantities we construct the total absorption coefficient:

$$\alpha(\lambda,\mathbf{r}) = \sum_{\mathbf{i}} \rho_{\mathbf{i}}(\mathbf{r})\kappa_{\mathbf{i}}(\lambda,\mathbf{r}) \qquad \text{in } cm^{-1} \qquad (3)$$

• The optical depth at wavelength λ from observer to a distance R is:

$$\tau(\lambda) = \int_0^R \alpha(\lambda,\mathbf{r})dr \text{ (dimensionless)} \qquad (4)$$

• The extinction, in magnitudes, is defined to be:

$$A(\lambda) = 2.5 \bullet \log_{10}(e)\, \tau(\lambda) = 1.086\ \tau(\lambda) \qquad (5)$$

The following quantities also appear frequently in discussions about dust:

$$E(\lambda_1 - \lambda_2) = A(\lambda_1) - A(\lambda_2) \qquad (6)$$

$$R_V = \frac{A_V}{E(B-V)} \qquad (7)$$

In Fig. 1 we plot $A(\lambda)/A(V)$ versus $x = \lambda^{-1}$ for 4 different values of R_V. The curves are drawn from analytical fits to large amounts of Galactic data, constructed by Cardelli, Clayton and Mathis (Cardelli 1989). These fits are represented by the equation:

$$\frac{A_\lambda}{A_V} = a(x) + \frac{1}{R_V} b(x) \qquad (8)$$

where $x=\lambda^{-1}$ (in μ^{-1}), and a(x), b(x) are two purely formal analytic functions with no direct physical significance. We shall make use of eq. 8 in later discussions.

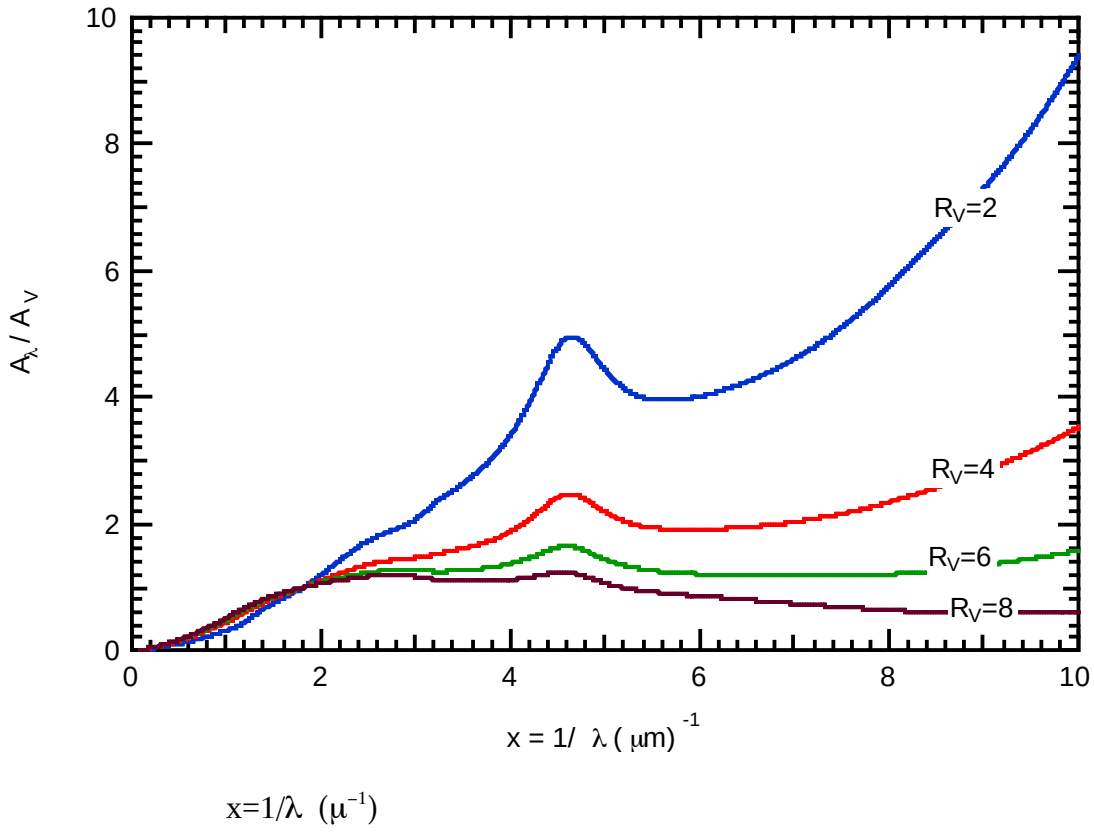

Fig.1 Four distinct curves for absorption by dust in our Galaxy.

A number of features related to Fig. 1 are very important:

• **The value of R_V depends on the environment along the line of sight.** A direction through a low-density interstellar medium (ISM) *usually* yields a low value: $R_V \approx 2$, while lines of sight through dense clouds give $R_V \approx 4$ to 6. (Unfortunately it is not possible to quantify precisely this very important correlation between R_V and dust density.) For low values of R_V, $A(\lambda)/A(V)$ varies strongly with x in the UV, while for larger values of R_V, the dependence of $A(\lambda)/A(V)$ on x in the UV is much weaker. Why? This is almost certainly due to the fact that in the interior of dense clouds, which are relatively well shielded from intense UV, various grain destruction mechanisms are diminished, and the growth of relatively large grains by coagulation is facilitated. Of course large grains have opacities that vary more slowly with x than small grains; this is a direct consequence of the theory of Mie scattering. One says that large grains are "grayer" than small grains. However, in the visible and especially in the IR, the dependence of $A(\lambda)/A(V)$ on R_V is not nearly as dramatic, as can be seen by inspection of Fig. 1 in the range $x < 2.5\ \mu^{-1}$.

•**The large bump in each curve of Fig.1 at $x=4.6\ \mu^{-1}$ ($\lambda=217$ nm) is almost certainly due to graphite** (and/or other stable forms of solid carbon that are spectroscopically similar). Laboratory experiments show a resonance in graphite at this wavelength with the required oscillator strength and line-width [Will, 1999]. Although it is not possible to see them in Fig.1, there are other significant resonances in the extinction curve. For example, in the visible there are ≈40 absorption bands, the strongest of which is at 443 nm. There are also strong emission bands in the NIR at 3.3, 6.2, 7.7, 8.6, and 11.3 μ. These wavelengths all correspond to C-H or C-C bond vibrations in aromatic hydrocarbons, which could occur as polycyclic aromatic hydrocarbons (PAHs- which are constructed of several benzene rings joined together in a plane), and/or as more complex aromatics. Bands at 9.7 and 18 μ are probably due to SiO_4 tetrahedra in more complex structures such as olivine: $(Mg, Fe)_2\ SiO_4$. A band at 3.1μ is probably water ice or ammonia ice.

•**How large is the absorption coefficient?** Roughly speaking, for the typical line of sight in our neighborhood of the Galaxy in B band, we have $\alpha_B \approx 3\text{-}4\ \text{kpc}^{-1}$.

•**What is the spatial distribution of Galactic dust?** From IRAS surveys at 100 μ and from a variety of other sources, we know that Galactic dust is concentrated in spiral arms where there is a relatively high rate of star formation, it has a scale height of about 100 pc normal to the Galactic plane in either direction, and it increases as one goes toward the Galactic center from the Sun's position at $\rho \approx 8$ kpc . There is some indication from the IRAS survey that the dust density reaches a maximum at $\rho \approx 4$ kpc, and then decreases to some extent for smaller r_0, reaching a local minimum at $\rho \approx 2$ kpc. (See Fig. 2).

•**What are the relative proportions of graphites, silicates, aromatic hydrocarbons, and ices; and what are the grain size distributions that account for all the observed features of Fig.1?** Unfortunately the solution to this problem is not unique- many different mixtures can account for the results of Fig.1. However, there is a "standard Galactic dust model" that most experts agree is the most plausible solution; [Weingartner 2001, Mathis 1990, Cardelli 1989, Draine 1984]. According to these authors, along a "typical" line of sight both graphite and silicate grains are distributed in size according to the formula:

$$dn_{grain} = C\ n_H\ a^{-3.5}\ da \qquad (9)$$

Here, for simplicity the grains are assumed to be spherical; C is a constant:

$C_{graphite}=10^{-25.13}$ cm$^{2.5}$ $\qquad$ $C_{silicate}=10^{-25.11}$ cm$^{2.5}$

n_H is the number density of H atoms, and a is the grain radius in cm, with a_{min}=50 Angstroms, a_{max} = 0.25 μ. Of course this "standard" model assumes that the dust density is everywhere proportional to the atomic hydrogen density, it ignores the spatial variations in size and composition that are well known to occur, and it also ignores the fact that many grains are not spherical, but rather elongated "needles" with large aspect ratios. The evidence for the latter is the well-known phenomenon of starlight polarization, caused by the alignment of elongated paramagnetic grains with the Galactic magnetic field. (It is also known from various laboratory experiments and theoretical analyses that crystal growth from the vapor phase is strongly favored at "screw-dislocation sites", and in this case long needle-like crystals tend to form [Frank 1949, Bacon 1960, Donn 1963, Sears 1955, Kittel 1986].) It is possible that the starlight polarization phenomenon could actually be used as a diagnostic to study host galaxy extinction of supernova light.

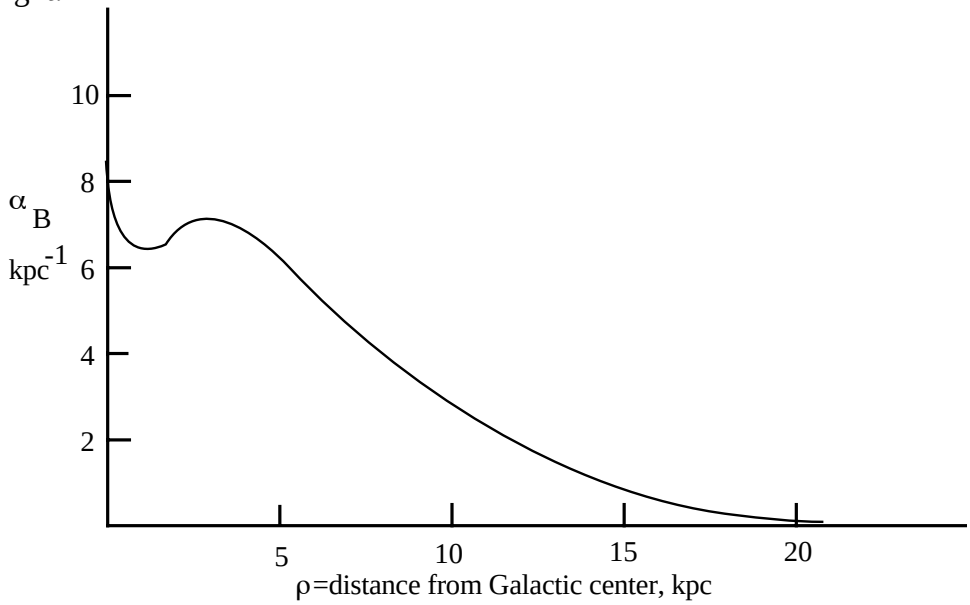

Fig.2. Rough sketch of the radial dependence of α_B in the Galactic plane.

One final and obvious remark about Galactic dust: It can lead to a systematic error in SN1a observations, but at least in the simplest approximation, this should not *weaken* the interpretation of cosmic acceleration. Distant SN1a radiate light that is red-shifted into optical bands for which Galactic extinction is relatively small, whereas the light from nearby SN1a is not so red-shifted, and thus suffers more extinction on entering the Galaxy on the way to detectors.

2. Basic facts about dust in other galaxies.

Although many detailed studies have been made of Galactic dust, there is comparatively little quantitative information about dust in other galaxies. Some information exists for the large and small Magellanic clouds (LMC,SMC); see for example [Pei 1992, Fitzpatrick 1999]. Here, the most important properties are summarized in Table 1, where Galactic properties are all normalized to unity:

Table 1. Comparison of Galaxy, LMC, SMC Dust Properties

PROPERTY	GALAXY	LMC	SMC
Dust to gas ratio	1	.2	.1
Heavy element abundance	1	.33	.13
Mass ratio of dust to neutral H	1	.25	.16
Strength of “graphite” peak	1	.5	.13
Far IR extinction	1	2	3

Although in the Galaxy, the observed extinction curve is reasonably well explained by assuming roughly equal numbers of silicate and graphite grains, the ratio of graphite to silicate is much smaller in the SMC, while the LMC is intermediate.

There exist a few quantitative studies of extinction for relatively nearby galaxies (distance < 10 Mpc) where it is possible to resolve individual stars.

Some recent observations with the Hubble Space Telescope (HST) by W.C. Keel and R.White [Keel 2001] make use of several spiral galaxies of low z, (each of which is backlit by an elliptical galaxy, see Fig.3) to reveal interesting properties of the spiral galaxy dust, even though in these cases individual stars are not resolved. By observing each galaxy in the regions free of overlap and by using symmetry, Keel and White infer the separate contributions of the luminosity of each galaxy that would occur in the overlap region, in the absence of dust. This is compared with the actual luminosity of the overlap region, and the difference is attributed to extinction by foreground galaxy dust. They find in each case that the dust is strongly confined to fairly narrow lanes associated with the spiral arms, just as in our Galaxy. In regions between the spiral arms, the dust density is low and the extinction is weak. These authors also find that in some cases the extinction curve is quite similar to that of our Galaxy (see Fig.1), whereas in some of the backlit spirals, the extinction curve has a weaker dependence on wavelength (is much “grayer”).

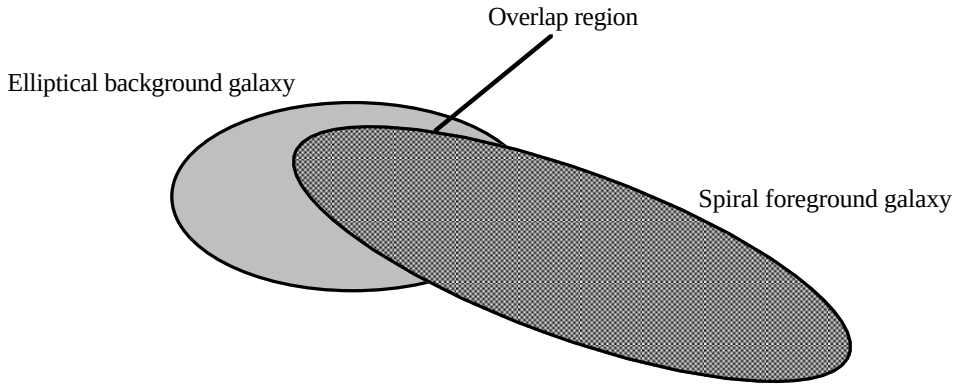

Fig.3. Schematic diagram illustrating the method of Keel and White [Keel 2001].

Falco et al [Falco 1999] studied the dust and extinction curves of 23 gravitational lens galaxies over the range $0 < z < 1$, and found a wide range of R_V values, extending from $R_V = 1.5 \pm 0.2$ for an elliptical at z=.96 to $R_V = 7.2 \pm 0.1$ for a spiral at z=0.68. Of course, we might expect R_V to be closer to unity for an elliptical galaxy, which has relatively little dust. At the opposite extreme a very dusty spiral would be *expected* to yield $R_V = 6$ or 7. However, we have no sure way to quantify the range of dust densities between these two extremes. Probably it spans at least 2 or 3 orders of magnitude, and possibly even 4.

As a very crude rule of thumb we expect that the dust density in any given galaxy, and therefore the absorption coefficient α should be roughly proportional to the star formation rate. Furthermore, we know that the global star formation rate at z=1 was approximately 6-10 times larger than it is now. Thus we expect that the typical large spiral or elliptical galaxy might have been considerably dustier at z=1 than it is today, although the most dramatic changes since z=1 have probably occurred in blue dwarf galaxies [Dressler 1999]. Unfortunately it seems impossible at present to translate this important but qualitative statement into something more quantitative and precise.

3. Basic facts about Intergalactic dust.

Aguirre [Aguirre 1999a,b, 2000] has proposed that the dimming of light from distant SN1a might be caused by extinction due to intergalactic (IG) dust, rather than by acceleration of the Hubble expansion. He has suggested that the usual test for the presence of dust- namely, reddening of starlight- might not be applicable to SN1a observations, because IG dust might be substantially grayer than normal galactic dust. In support of this contention he has proposed the following scenario:

IG dust is created in galaxies, along with the dust that remains there. However, a portion of the galactic dust is driven out of a typical galaxy by radiation pressure. The larger, longer needle-like grains are most affected by this radiation pressure, they are the ones least susceptible to destruction by sputtering, and it is precisely these grains that have the "grayest" opacity. Crude but at least superficially plausible order-of magnitude estimates by Aguirre suggest that the radiation pressure would be sufficient to fill the space between galaxies with dust more or less uniformly in a reasonable time; and radiation transport calculations by Aguirre and Haiman suggest that the needle-like dust can account for the observed dimming of SN1a, without violating other observational constraints. In Sec.8 of these notes, we repeat the latter calculations in detail and extend them.

For the present, however, we merely ask: is there any observational evidence in support of Aguirre's suggestion? The fact is that the existence of IG dust has never been solidly established and there are only upper limits on its absorption coefficient. For example, it has been suggested that X-ray halos might be generated from scattering, by diffuse IG dust, of X rays originating in well defined remote sources. Predehl and Klose [Predehl 1996] have carried out a detailed study of such halos, and obtain an upper limit of $\approx 10^{-4}$ magnitudes/Mpc on the IG absorption coefficient, comparable to an older limit obtained by optical means. For a supernova at z=1, this limit would correspond to a maximum extinction of $\approx .25$ magnitudes, (at rest frame *X-ray* wavelengths, to be sure!) It might be possible to refine this limit in the future.

4. Host galaxy extinction of SN1a. Basic method.

In the next few sections we want to understand in some detail how host galaxy extinction might lead to a significant systematic error in the interpretation of SN1a observations. For such an error to occur, it is obvious that host galaxy extinction must depend on z. Furthermore, to weaken the conclusion that the Hubble expansion is accelerating, the extinction must *increase* with z. In what ways can host galaxy extinction be z dependent?

• As suggested at the end of section 2, the spatial distribution and/or physical character of the dust in any given galaxy might well have evolved over billions of years, and extinction may have been considerably greater at z=1 than for z≈0, possibly by an order of magnitude in some galaxies.

• Quite apart from evolution, observational selection leads to a z dependence of host galaxy extinction, because, for any assumed values of Ω_m and Ω_Λ, the apparent magnitude m of a standard SN1a increases as z increases. Now, there is a limiting $z=z_0$ corresponding to a maximum apparent magnitude m_0 beyond which one cannot observe a SN1a reliably. For SNAP it appears that $z_0 \approx 1.7$. For the 42 supernovae in the $z \approx .5$ range that yield the important conclusions described in [Perlmutter 1999] $z_0 \approx .85$. For the nearby supernovae analyzed by Guillaume Blanc, $z_0=0.3$. As z approaches z_0 from below, we can tolerate less and less extinction from host galaxy dust before we reach m_0. To put this on a quantitative basis, we recall the magnitude red-shift relation, derived from Friedmann's second equation. Assuming that $\Omega_m + \Omega_\Lambda = 1$, this may be written:

$$m = M + 5\log_{10}\left[(1+z)\int_0^z \frac{dx}{\sqrt{1+x\left(x^2+3x+3\right)\Omega_m}}\right] + C \qquad (10)$$

where M is the absolute magnitude of a standard SN1a and C is a constant. (Here x is just a dummy variable of integration). Now, let A_0 be the limiting extinction which at $z < z_0$ increases the magnitude m to m_0:

$$A_0 = m_0 - m \qquad (11)$$

Then from (10) we obtain:

$$A_0 = 5\log_{10}\left[\frac{(1+z_0)\int_0^{z_0} \frac{dx}{\sqrt{1+x\left(x^2+3x+3\right)\Omega_m}}}{(1+z)\int_0^{z} \frac{dx}{\sqrt{1+x\left(x^2+3x+3\right)\Omega_m}}}\right] \qquad (12)$$

We have evaluated this expression numerically. To a very good approximation, we find:

$$A_0\left(\Omega_m = .3, \Omega_\Lambda = .7\right) = 2.33\, ln\left(\frac{.3}{z}\right), \quad \mathbf{z_0} = .3$$

$$= 2.48\, ln\left(\frac{.85}{z}\right), \quad \mathbf{z_0} = .85 \qquad (13)$$

$$= 2.57\, ln\left(\frac{1.7}{z}\right), \quad \mathbf{z_0} = 1.7$$

and:

$$A_0\left(\Omega_m = 1, \Omega_\Lambda = 0\right) = 2.23\, ln\left(\frac{.3}{z}\right), \quad \mathbf{z_0} = .3$$

$$= 2.29\, ln\left(\frac{.85}{z}\right), \quad \mathbf{z_0} = .85 \qquad (14)$$

$$= 2.34\, ln\left(\frac{1.7}{z}\right), \quad \mathbf{z_0} = 1.7$$

Note that there is very little difference between formulae 13 and the corresponding formulae 14.

5. Host galaxy extinction. The model of Hatano, Branch, and Deaton.

Now we are in a position to discuss detailed models of host galaxy extinction. We want to employ a computer model simple enough to use and interpret, but sophisticated enough to take into account the relevant facts. In addition to various facts about dust and observational selection already mentioned, the following are also important:

• SN1a often occur in spiral arms of spiral galaxies. However, they also occur in "old" populations, for example in bulges of spiral galaxies and in elliptical galaxies.

• There is some evidence that SN1a from inner portions of spiral arms are slightly brighter (by 0.2 –0.3 magnitudes) than those originating in outer portions of spiral arms or in elliptical galaxies. However, once the stretch factor is taken into account, this residual variation of brightness with location or galaxy type disappears (at least at the present level of precision).

Taking all this into account, we find that a good starting point is the model proposed by Hatano, Branch, and Deaton [Hatano 1998], hereafter (HBD). This is a Monte Carlo calculation of $A_{B,\ \text{rest frame}}$ for a simple axially symmetric model of a disc galaxy with a central bulge. The supernovae are assumed to be placed in 2 distinct distributions: (and where all lengths are in kpc):

• A spherically symmetric bulge distribution with supernova density proportional to

$$\frac{1}{R^3 + 0.7^3} \qquad (15)$$

where R is the radial distance from the origin in spherical coordinates, and we assume the distribution is truncated at R=3;

• An axially symmetric disc distribution with density proportional to:

$$e^{-r_0/5}e^{-|z_0|/0.35} \qquad (16)$$

The disc SN1a are assumed to outnumber those in the bulge by a factor of 7. (Note that the characteristics of bulges vary widely from one spiral galaxy to another; hence the choice of bulge parameters given here is somewhat arbitrary. However the results do not depend very much on whether or not the bulge contribution is included).
The dust is assumed to have an axially symmetric distribution with a vertical scale height of 0.1 kpc, and the following radial distribution of absorption coefficient α_B:

$$\begin{aligned} \alpha_B(\rho) &= \rho \qquad && 0 \le \rho \le 5 \text{ kpc} \\ \alpha_B(\rho) &= 7 - 0.4\rho \qquad && 5 \le \rho \le 17.5 \text{ kpc} \end{aligned} \qquad (17)$$

This simple model is consistent with the rough sketch of α_B given in Fig.2.

6. Features of our calculations of host galaxy extinction.

We have constructed a computer code: "Host extinction.F" to verify and extend HBD. In this section we describe some of the essential features of our code; then in following sections, we present the results.

• **Geometry.**

Fig. 4 shows the geometry used for calculating extinction due to the host. We assume an axially symmetric galaxy with origin at O. Consider a plane parallel to the galactic plane, but displaced from it by a distance z_0 (O'O=z_0). Let P be the location of the supernova in that plane, at radial distance r_0 from O'. Let PP' be a vector directed toward the observer. PP' is inclined by angle θ with respect to the normal to the galactic plane. Let the projection of PP' in the plane be PQ, of length r. Construct the diameter AB through O' that is parallel to PQ. Then the plane polar coordinates ρ, z of a small element of dust are given by:

$$\begin{aligned} \rho &= \sqrt{r^2 + r_0^2 - 2rr_0\cos\beta} \\ &= \sqrt{R^2\sin^2\theta + r_0^2 - 2Rr_0\sin\theta\cos\beta} \end{aligned} \qquad (18)$$

and

$$z = z_0 + R\cos\theta \qquad (19)$$

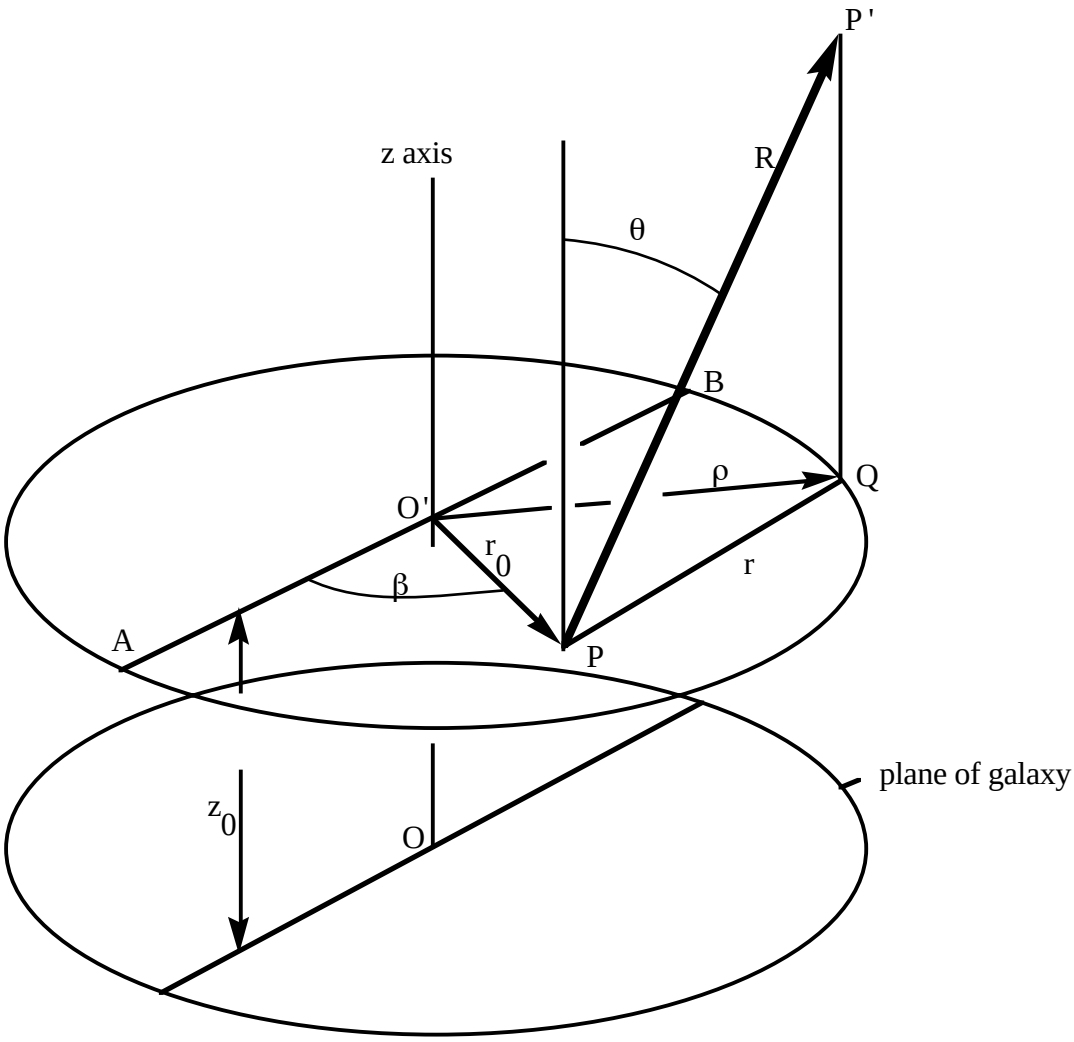

Fig.4.

Given the location of the supernova at P= (r_0, z_0, β), the inclination angle θ, and the extinction coefficient α as a function of ρ, z, we use equations 5,18, and 19 to calculate the extinction:

$$A_B = 1.086\int_0^\infty \alpha_B(\rho,z)dR \qquad (20)$$

by numerical integration. The Monte Carlo portion of the calculation enters in the random choice for supernova location (point P), taking into account the probability distribution for this location.

• **Distribution functions in our code.**

Model #1: In our code, the supernova bulge distribution is identical to that of HBD, and the disc supernova distribution is given by:

$$f(r_0) = const \bullet exp(-r_0 / 5) sec\, h^2(3z) \qquad (21)$$

This is almost the same as that of HBD, except that the z dependence is smoother than in HBD. As in HBD we assume that 7 times as many supernovae appear in the disc as in the bulge. As for the dust distribution, it is identical to that of HBD except that it is multiplied by an overall "absorption coefficient factor" b that can be chosen anywhere over a wide range. We have done calculations for b in the range 0.01 to 100, with most attention paid to the values between b=0.1 and 10.

Model #2 : The supernova distributions are the same as in Model #1, but the dust radial distribution is a Gaussian with no minimum at ρ=0:

$$\alpha_{\mathbf{B}}(\rho) = 6 exp(-.0064\rho^2) \qquad (22)$$

In the region 5 <ρ < 15, the absorption coefficients in models 1 and 2 are very nearly identical. Just as in Model #1, here we also employ the factor b. Actually, we have used Model #2 for most of our calculations.

• **Filters; rest frame vs. observer frame colors; color excesses.**

The wavelength dependence of host galaxy extinction is an important issue that must be considered carefully. To approach this problem it is essential at the very outset to choose for our discussion an appropriate set of optical and infra-red filters. A very convenient and sensible choice has been suggested by Alex Kim, who pointed out that K-correction errors are minimized if one chooses filters with peak-transmission-wavelengths λ_n that satisfy the relation:

$$\lambda_{n+1} = 1.15\lambda_n \qquad (23)$$

For some of our calculations, we thus choose the following 10 peak-transmission -wavelengths:

Table 2 Peak transmission wavelengths of 10 selected filters

λ_1=445 nm (B-band)	λ_2=1.15 λ_1 = 512 nm
λ_3=1.15 λ_2 = 589 nm	λ_4=1.15 λ_3 = 677 nm
λ_5=1.15 λ_4 = 778 nm	λ_6=1.15 λ_5 = 895 nm
λ_7=1.15 λ_6 = 1029 nm	λ_8=1.15 λ_7 = 1184 nm
λ_9=1.15 λ_8 = 1361 nm	λ_{10}=1.15 λ_9 =1565 nm

Suppose that in the rest frame, light is emitted at one of these wavelengths: λ_n, and suppose also that this light is observed at wavelength λ_{n+m} where m=0,1,2,3,… Then we have:

$$1+z = 1.15^m$$

or:

$$z = 1.15^m - 1 \qquad (24)$$

For future reference, we tabulate the transformation of rest-frame to observer wavelengths for z given by eq. 24 with m=0,…, 7 as follows:

Table 3. Transformation of rest frame to observer wavelengths for the filters of Table 2.

z =	**0.0**	**.15**	**.32**	**.52**	**.75**	**1.01**	**1.31**	**1.66**
1 →	**1**	**2**	**3**	**4**	**5**	**6**	**7**	**8**
2 →	**2**	**3**	**4**	**5**	**6**	**7**	**8**	**9**
3 →	**3**	**4**	**5**	**6**	**7**	**8**	**9**	**10**
4 →	**4**	**5**	**6**	**7**	**8**	**9**	**10**	
5 →	**5**	**6**	**7**	**8**	**9**	**10**		
6 →	**6**	**7**	**8**	**9**	**10**			
7 →	**7**	**8**	**9**	**10**				
8 →	**8**	**9**	**10**					
9 →	**9**	**10**						

It will be convenient to focus our attention on the 8 red-shifts listed in this table, when we discuss some of our results. We must also take into account the relation between color excess and extinction. For this purpose we recall eq'n (8):

$$Q_{\lambda V} \equiv \frac{A_\lambda}{A_V} = a(x) + \frac{1}{R} b(x) \qquad (25)$$

where a(x), b(x) are the functions determined by Cardelli, Clayton and Mathis; $x=1/\lambda$ (in μ^{-1}), and $R^{-1} = A_B/A_V - 1$. Now,

$$Q_{\lambda\lambda'} = \frac{A_\lambda}{A_{\lambda'}} = \frac{A_\lambda}{A_V}\frac{A_V}{A_{\lambda'}} = \frac{Q_{\lambda V}}{Q_{\lambda' V}}$$

and

$$E(\lambda,\lambda') = A_\lambda - A_{\lambda'} = A_\lambda\left(1 - \frac{Q_{\lambda' V}}{Q_{\lambda V}}\right)$$

Hence,

$$E(\lambda,\lambda') = A_B \frac{E(\lambda,\lambda')}{A_\lambda}\frac{A_\lambda}{A_B} = A_B \frac{Q_{\lambda V} - Q_{\lambda' V}}{Q_{BV}} \qquad (26)$$

Using (26) and a(x) and b(x) from Cardelli, Clayton, and Mathis, we can tabulate $E(\lambda_n, \lambda_{n+m})/A_B$ for m=1,…,7. These values will be used to calculate the color dependence of extinction.

• **Fundamental uncertainties**

What are the most significant uncertainties that one faces in attempting to calculate the effects of host galaxy extinction? Obviously they are as follows:

a) Dust absorption coefficients in other galaxies are unknown. Evolutionary effects could be very important. All we can do is to assume that the absorption coefficient determined for this local region of our Galaxy is somehow representative, as is its spatial distribution. We know that galaxies at z≈1 may have have been dustier than they are now, but we don't know by what factor. The only thing we can do is to guess, and parameterize our guess by the multiplicative "absorption coefficient factor" b already described.

b) We do not know how to describe the relationship between dust density and R_V with any precision. It appears that R_V increases with dust density, but we do not know whether the relationship is logarithmic, or some fractional power law, or something much more complicated. We shall simply make the following crude guess:

$$R_V = 3.5 \bullet b^{.16} \qquad (27)$$

This formula yields the following values, which look "reasonable" but could be very wrong.

Table 4. Assumed relationship between b and R_V

b	**R_V**
.01	**1.67**
.03	**2.0**
.1	**2.42**
.3	**2.89**
1	**3.5**
3	**4.17**
10	**5.05**
30	**6.03**
100	**7.31**

6. Results of our calculations of Host Galaxy extinction.

6.1 *Dependence on inclination angle* θ.

Fig.5 shows the results of a Monte Carlo calculation for 10,000 SN1a, using Model #1 with absorption coefficient parameter b=1 (Standard dust density) and inclination angle θ=0 (galaxy face on). We plot the probability distribution p(A) versus extinction A (rest frame B band), in the form of a histogram with bin width 0.05 magnitudes. We see that p(A) has a sharp peak at A≈ 0 but also a fairly long tail extending to large values of A. This is quite typical.

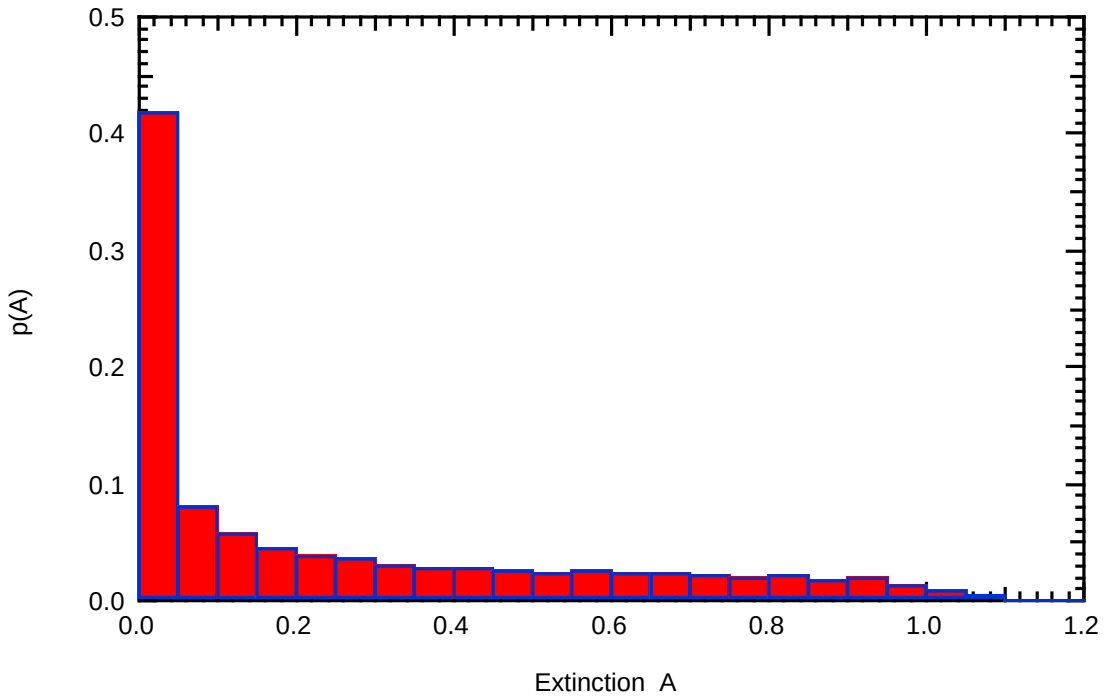

Fig.5. Probability distribution p(A) versus A, for θ=0. Model #1, b=1.0. (10000 SN1a.)

The origin of the sharp peak at A≈0 and of the long tail in Fig.5 are intuitively clear: A supernova located at or near the "surface" of the galaxy closest to the observer emits light that encounters little or no dust on its path to the observer (peak at A≈0); but light from a supernova in the interior of the galaxy, or on the far side, must pass through a substantial amount of dust (long tail). It is quite obvious that if we increase θ, the peak at A≈0 must decrease, and the tail must extend to larger values of A. We could show this quantitatively by plotting additional histograms, but it is more convenient to plot instead the cumulative probability P(A) that light from a supernova suffers extinction less than or equal to a given A. The relationship between P(A) and p(A) is:

$$P(A) = \int_0^A p(A')dA' \qquad (28)$$

In Fig.6. we plot P(A) versus A for several different inclination angles, and for cos θ distributed uniformly and randomly between 0 (galaxy edge on) and 1 (galaxy face on). Note the similarity of the curves for the latter case and for $\theta=60^{\cdot o}$. This is not at all surprising, since the average value of cos θ in a uniform distribution of that quantity between 0 and 90^o is 1/2.

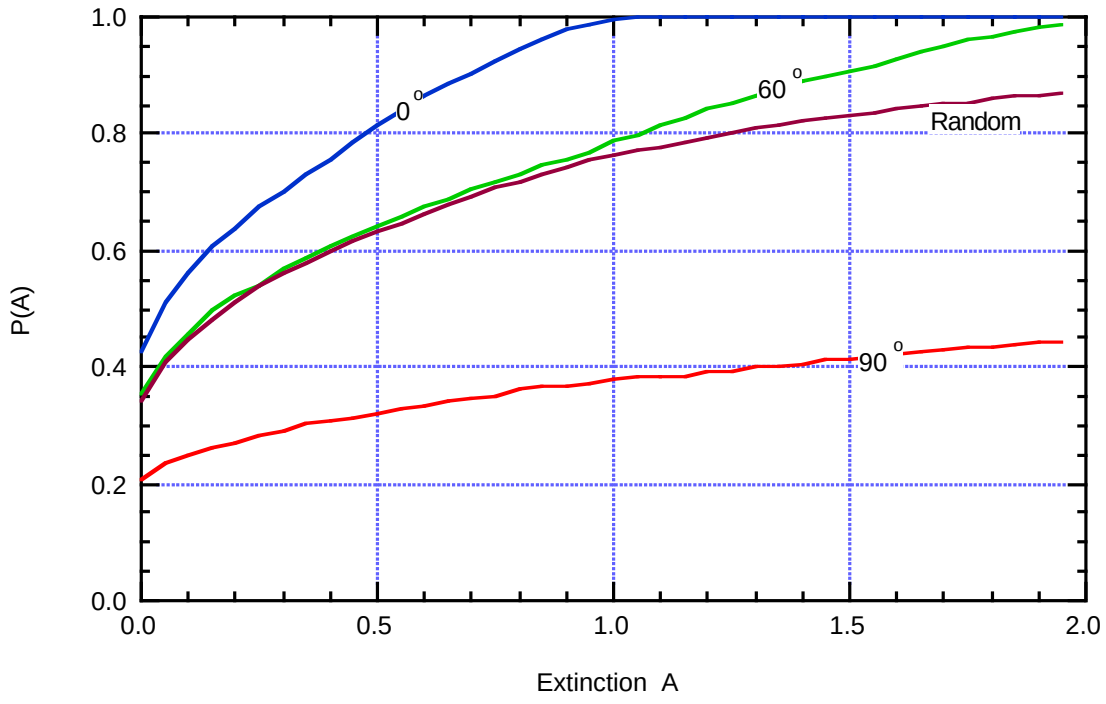

Extinction A

Fig. 6 Probability P(A) that a supernova has extinction less than or equal to extinction A plotted versus A. Blue: $\theta=0^o$, Green: $\theta=60^o$, Red: 90^o ; Purple: cos θ uniformly and randomly distributed between 0 and 1.

6.2 *Dependence of Observation Probability and Average Extinction on Projected Distance from Center of Galaxy.*

Let's consider the projected distance of a supernova from the center of the galaxy as viewed by an observer, when the inclination angle is θ and the azimuthal angle is β, (see Fig. 4). Ignoring a small correction arising from z_0 (the z coordinate of the supernova relative to the galaxy median plane), the projected distance r_P is found to be:

$$r_P = \sqrt{1 - \sin^2\theta \cos^2\beta} \qquad (29)$$

Fig.7 shows the results of 2 Monte Carlo calculations (Model #1, Model #2) each employing 1000 supernovae with b=1, and cos θ distributed uniformly and randomly from 0 to 1. The probability $P(r_p)$ to observe a supernova versus r_p is calculated and displayed as a histogram with bin width 2 kpc. Here, the results for Model #1 and for Model #2 are essentially identical; hence only a single histogram is shown. We also calculate the <u>average extinction</u> associated with each r_p bin. Here, the results are not at all surprising: Model #1 (essentially identical to that of HBD) assumes that the dust absorption coefficient goes to zero at the origin (recall eq. 17); therefore we expect somewhat less average extinction at very small r_p in that case. On the other hand Model #2 employs a Gaussian dust distribution with no minimum at the origin (see eq. 22). From now on we shall employ Model #2 exclusively, since it is "more conservative" (gives slightly more extinction).

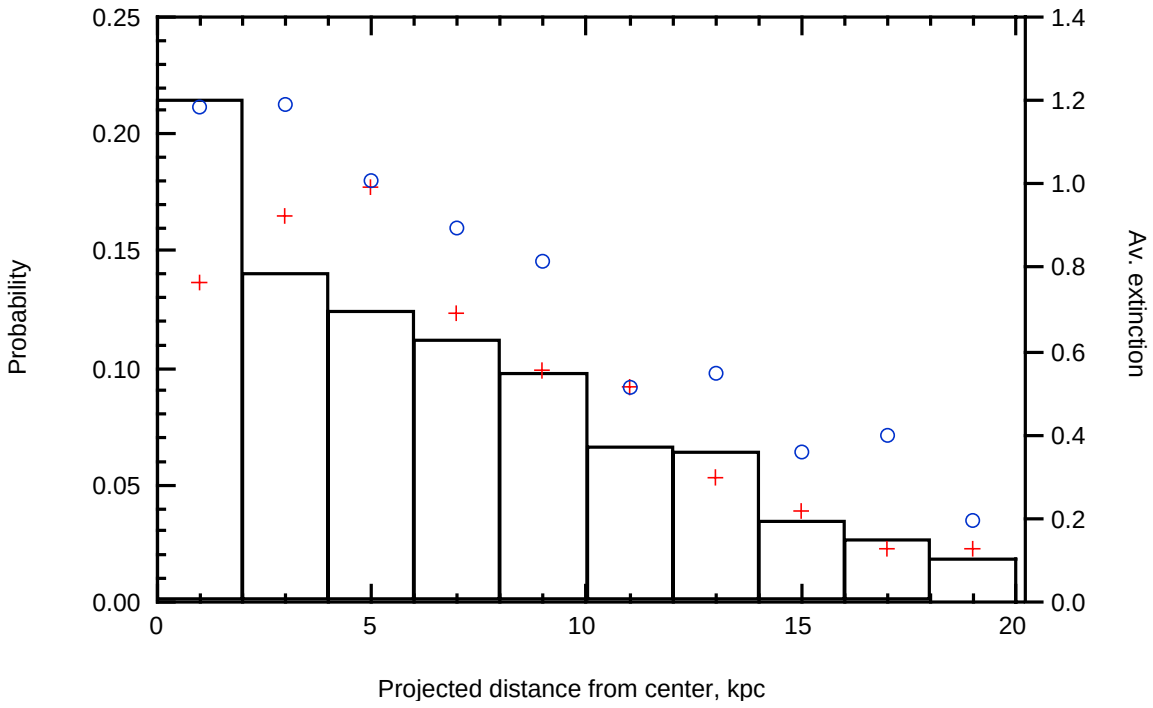

Fig.7 The histogram shows the probability to observe a supernova at projected radius given by abscissa, for Model #1 or Model #2 (left hand ordinate scale). Right hand scale: Open blue circles: Average rest frame B-band extinction for Model #2; red crosses: average rest frame B-band extinction for Model #1. For all calculations here, cos θ uniformly and randomly distributed between 0 and 1, and b=1.0.

6.3 *Dependence on Absorption Coefficient Parameter b and limiting redshift.*

Fig.8. shows the cumulative probabilities P(A) for 7 separate values of b: 0.1, 0.2, 0.4, 0.8, 1.6, 3.2, and 6.4 in 5000 point Monte Carlo calculations using Model # 2 with cos θ uniformly and randomly distributed between 0 and 1. Of course it is very easy to understand the qualitative trend of these curves: when b is small the dust density is low, and most supernovae have very little extinction. However, as b increases, fewer supernovae have low extinction and more have high extinction.

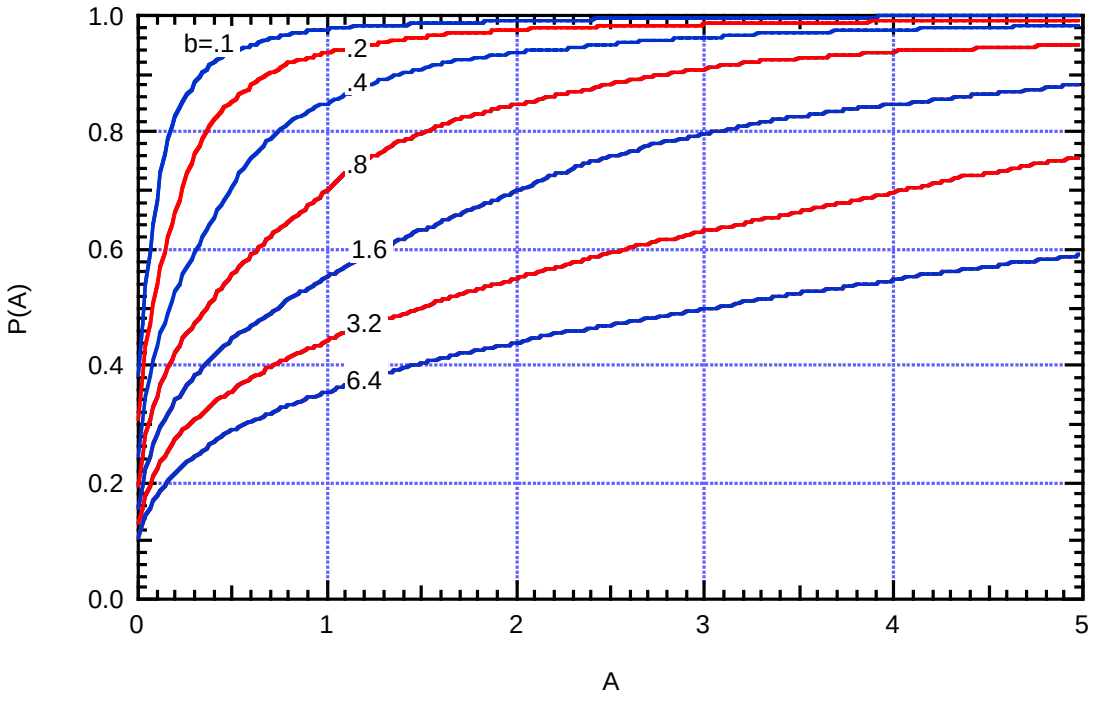

Fig. 8. Cumulative probability P(A) versus B-band rest frame extinction A, for:
b=0.1, 0.2, 0.4, 0.8, 1.6, 3.2, and 6.4.

Let's now recall that if there is a limiting red-shift z_0 beyond which supernovae observations cannot be made reliably, then at any given red-shift $z < z_0$, there is a limiting extinction A_0 which is given to a good approximation by formulae 13 or 14. We now combine results like those shown in Fig. 8 with the first of formulae 14 (Ω_m=1, Ω_Λ=0) to obtain additional results, shown in the next figure. Here (Fig. 9a) for various values of b, we plot versus z the probability $P(A_0)$ to observe a supernova with extinction less than or equal to the limiting extinction A_0, for z_0=.3, using Model #2. We see that for each value of b, $P(A_0)$ decreases as z approaches z_0 from below. The reason is simple of course: the closer z gets to z_0, the smaller the value of A_0, and the fewer supernovae exist with extinction less than A_0. Results are very similar for Ω_m=.3, Ω_Λ=.7. In Figs. 9b,9c, we make similar plots for z_0= 0.85 and 1.70, respectively.

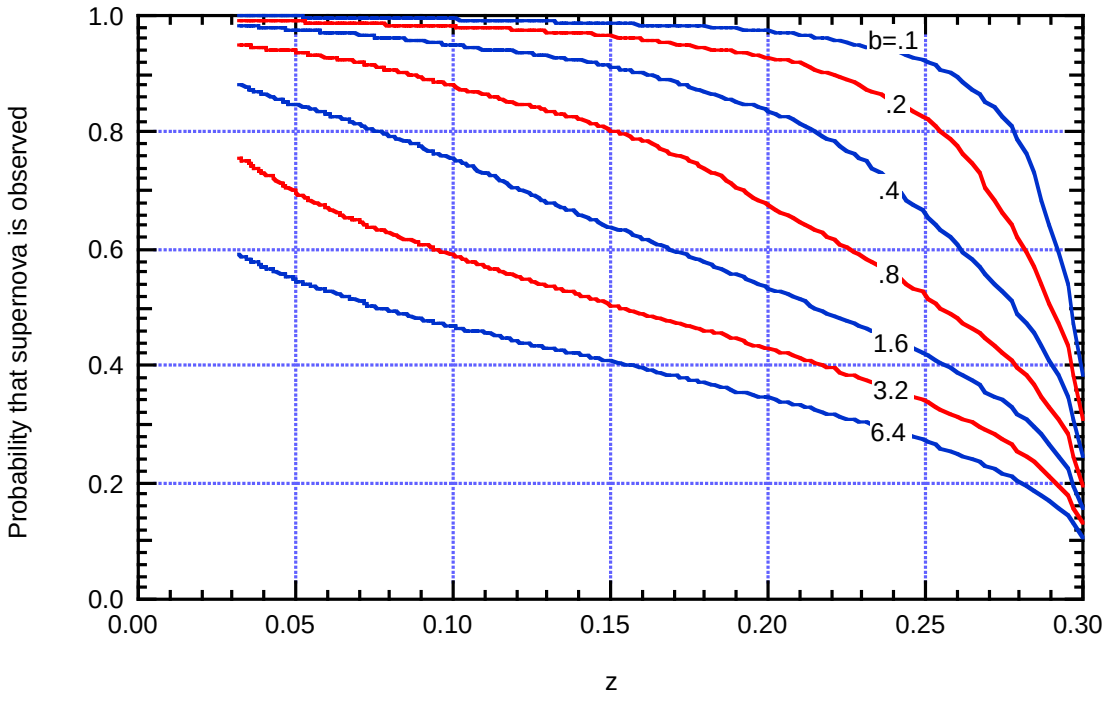

Fig.9a. Probability $P[A_0(z,z_0)]$ that a supernova has extinction less than or equal to A_0, versus z for z_0=0.3. Curves are plotted for b=.1, .2, .4, .8, 1.6, 3.2, and 6.4. Here cos θ is uniformly and randomly distributed between 0 and 1, and we employ Model #2.

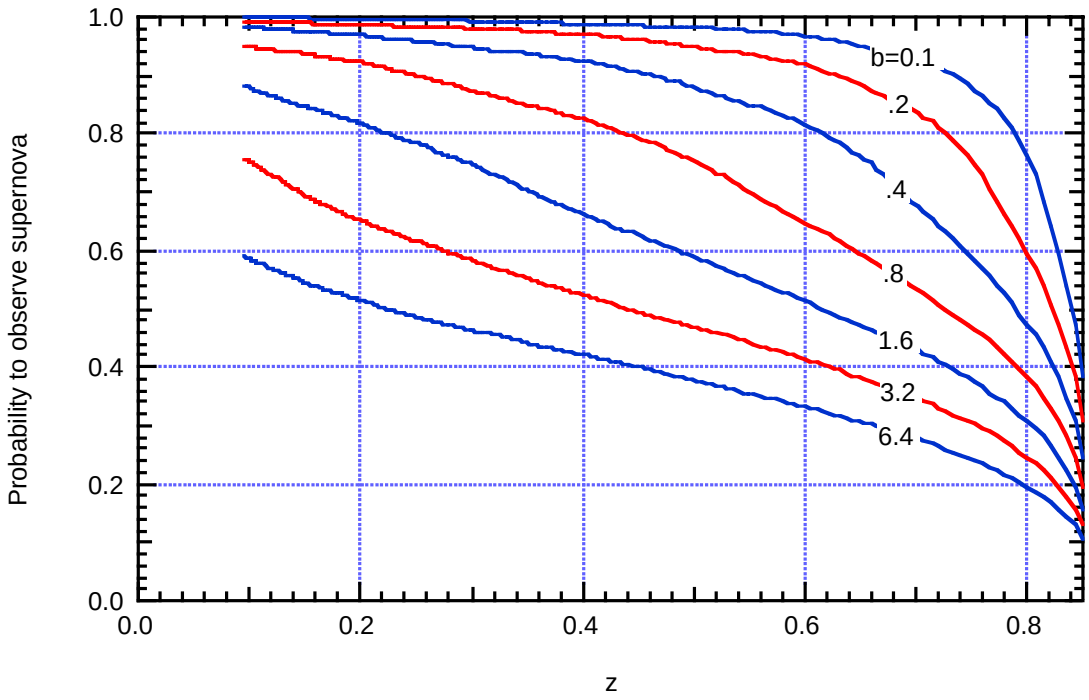

Fig.9b Same as Fig. 9a, but z_0=0.85

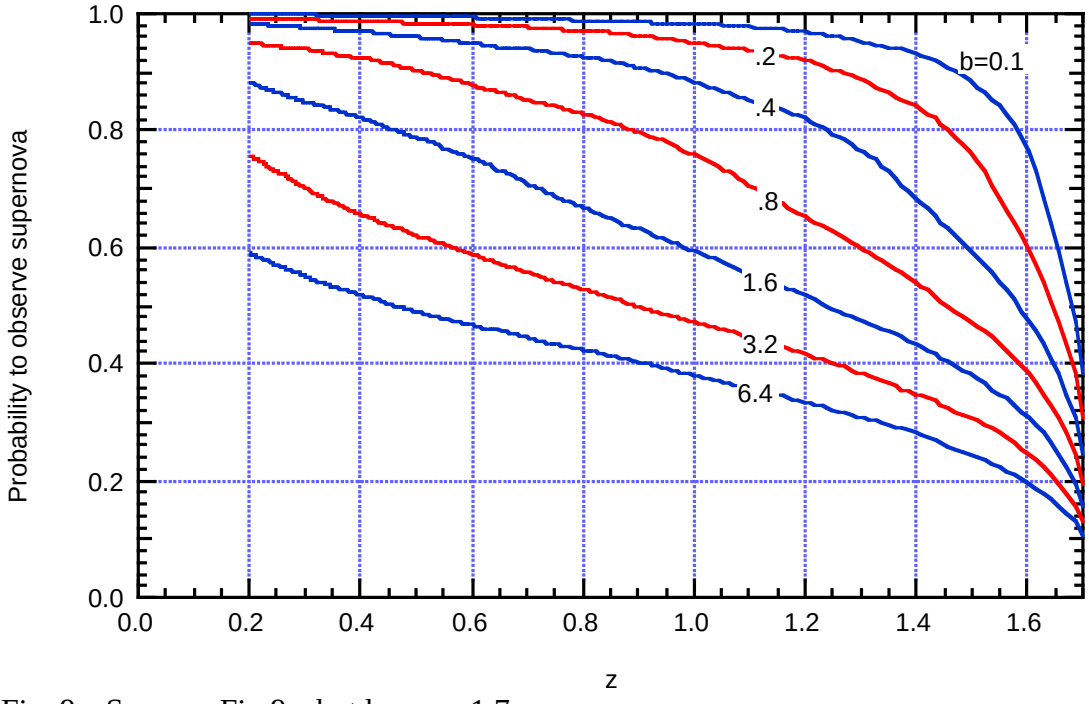

Fig. 9c Same as Fig 9a, but here z_0=1.7.

In Fig. 10a we plot the <u>average extinction</u> of all observable supernovae as a function of z, for different values of b, when z_0=0.3, and we employ Model # 2 (the same conditions as for Figs. 8 and 9a). Note that for z ≥ .15, <A> is the same for all b ≥ 0.8; while for z ≥ .20, <A> is the same for all b ≥ 0.4; and so forth. In other words, <A> "saturates" as b is increased. Furthermore, as z increases for fixed z_0, saturation of <A> occurs at a lower value of b. The same is true of the dispersion in A. Similar curves are shown in Figs 10b,c for z_0 = 0.85, 1.70 respectively.

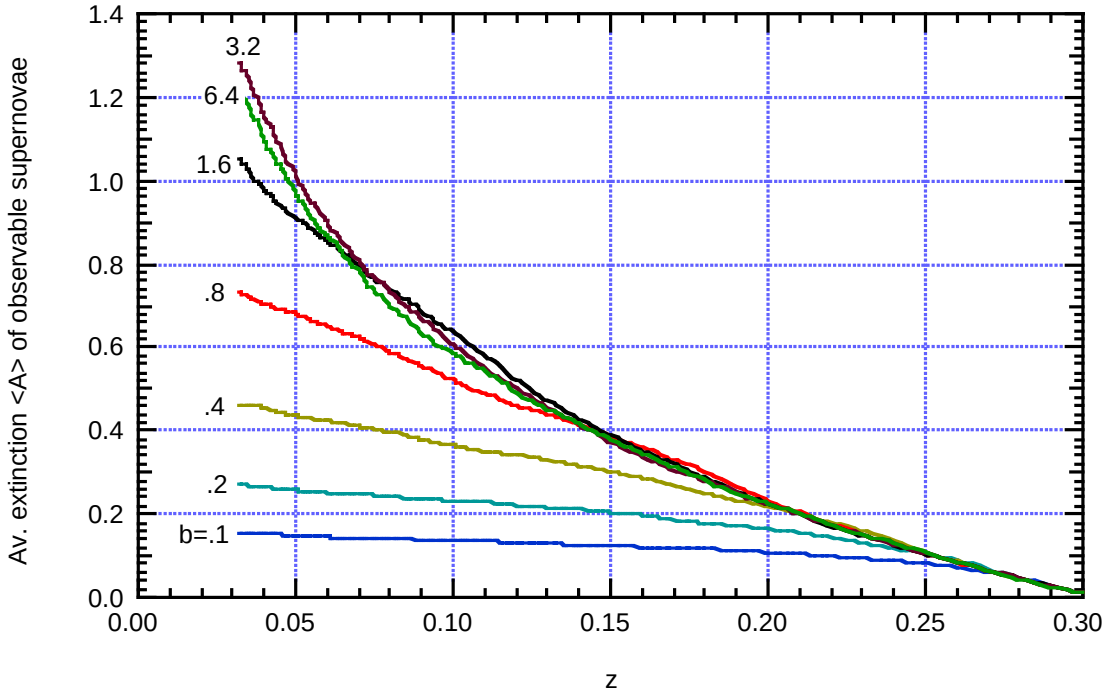

Fig. 10a Average extinction <A> of all observable supernovae, for various b values, as a function of z when z_0=0.3.

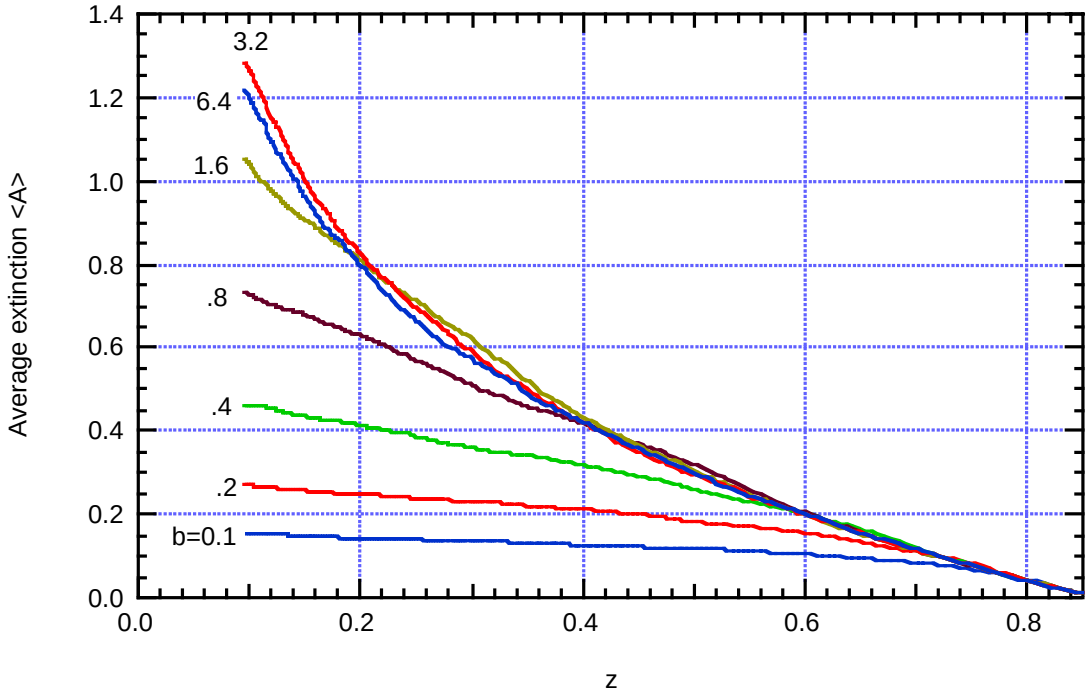

Fig. 10b Average extinction <A> of all observable supernovae, for various b values, as a function of z when z_0=0.85.

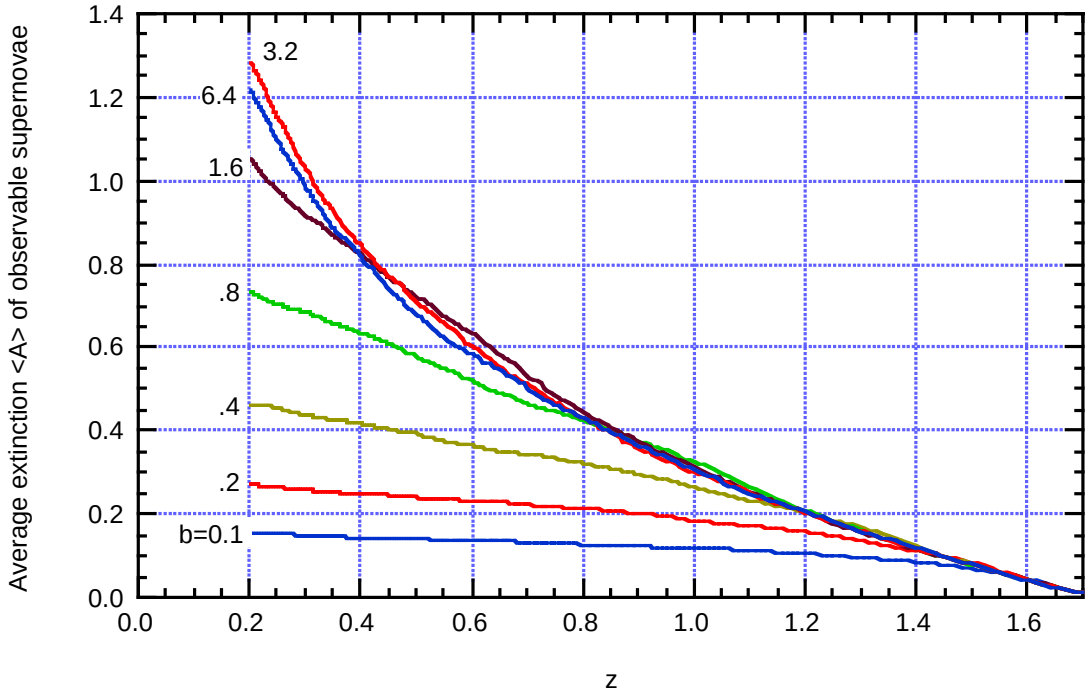

Fig. 10c Average extinction <A> of all observable supernovae, for various b values, as a function of z when z_0=1.70.

The saturation phenomenon can be seen in another way: For fixed z, we calculate the average extinction of all observable supernovae (those with extinction less than A_0):

$$< A >= \sum_{i=0}^{A_0} A_i p(A_i) \qquad (30)$$

and we also calculate the dispersion:

$$\Delta = (<A^2> - <A>^2)^{1/2} \qquad (31)$$

The results for z_0=0.85, z=.50 (with Model #2, Ω_m=1, and cos θ uniformly and randomly distributed from 0 to 1) are shown in Fig. 11.

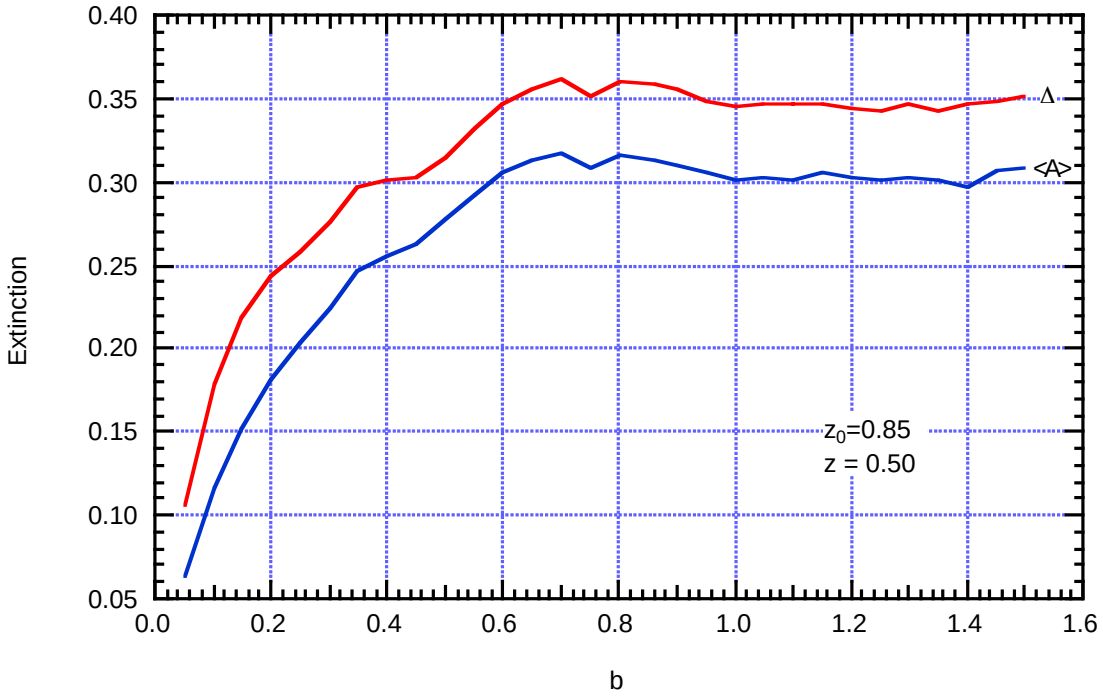

Fig. 11 Average extinction <A> and dispersion in extinctions Δ plotted versus b for z_0=0.85, and z=.50.

Fig. 12 is a plot of the saturating b value (blue), the saturated <A> (red), and the saturated Δ (green) versus z/z_0 for z_0=0.85 and Model #2. Fig. 13 is a similar plot except that the projected distance of all supernovae from the galactic center is constrained to be ≥ 6 kpc. As is expected, saturation occurs at larger values of b in the latter case, but the saturated <A> and Δ values remain essentially the same. Fig. 14 represents the results obtained when this projected distance is once again unconstrained, but the dust scale height is increased from its normal value of 100 pc to 330 pc. Finally Fig. 15 shows the results when the dust scale height is only 33 pc.

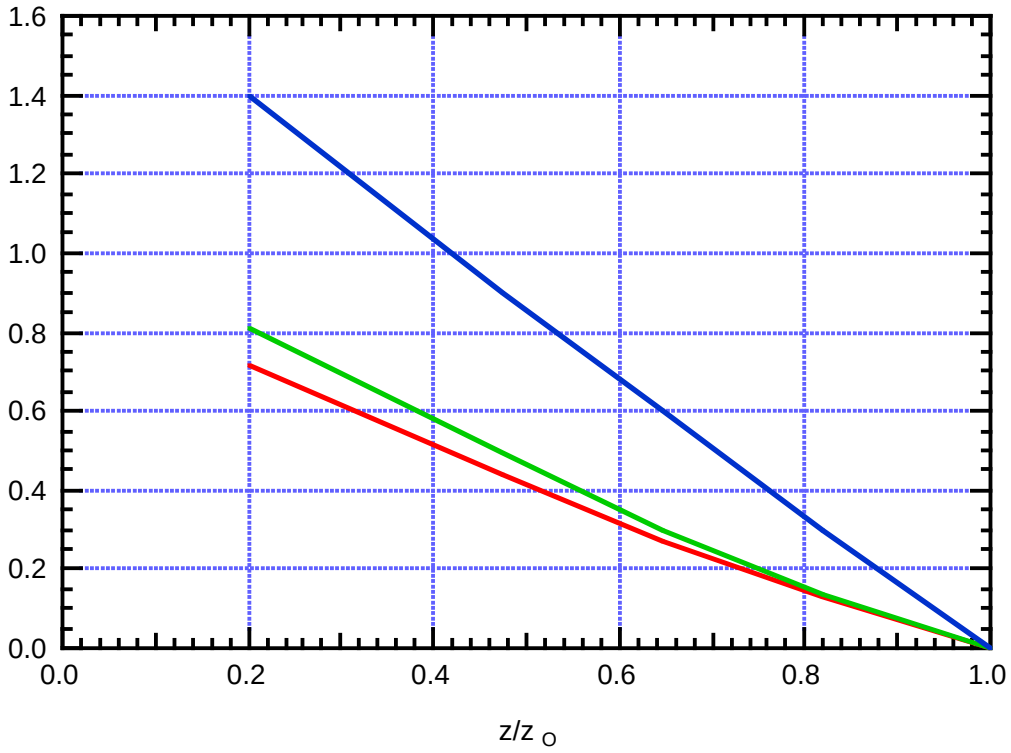

Fig.12 The saturation b value (blue curve), the saturated <A> (red curve), and the saturated Δ (green curve) for z_0=0.85 (Model #2, Ω_m=1, cosθ uniformly and randomly distributed between 0 and 1).

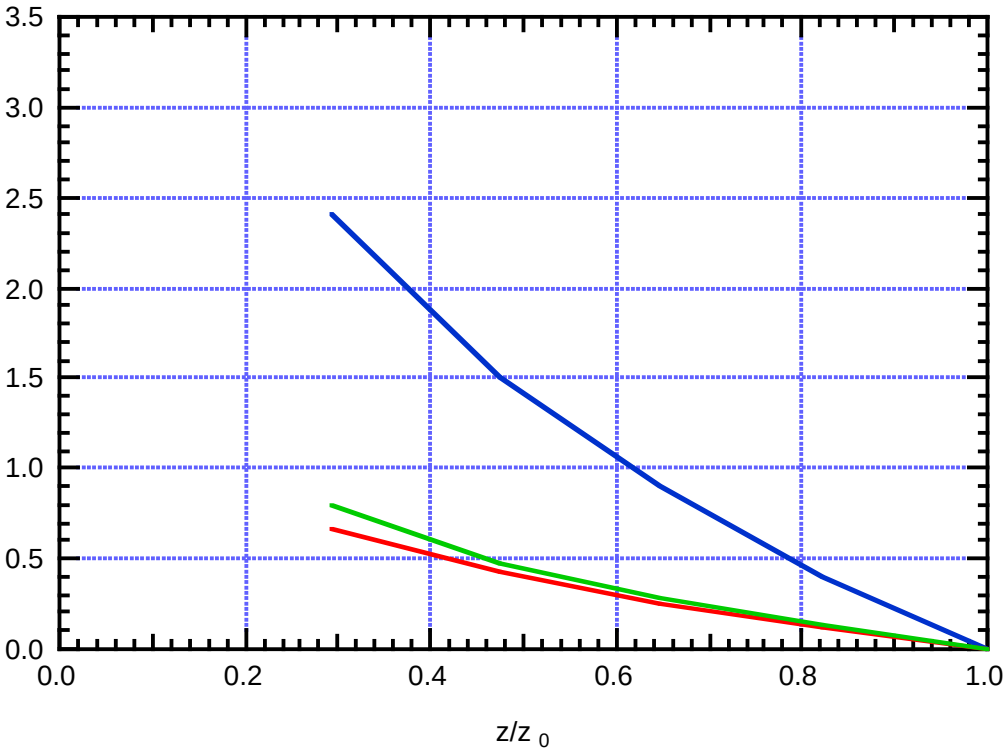

Fig. 13. z_0=0.85 as in Fig. 12, but projected radial distance of supernovae from galactic center constrained to be greater than or equal to 6 kpc.

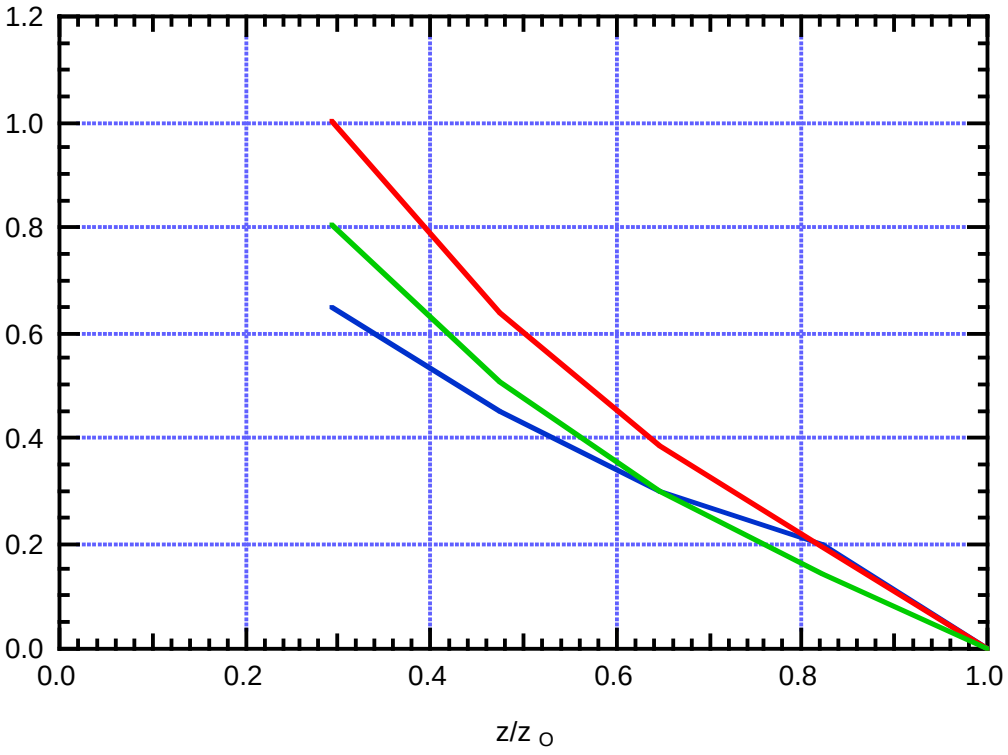

Fig. 14 Same as Fig. 12, but scale height of dust perpendicular to galactic plane is 330 pc.

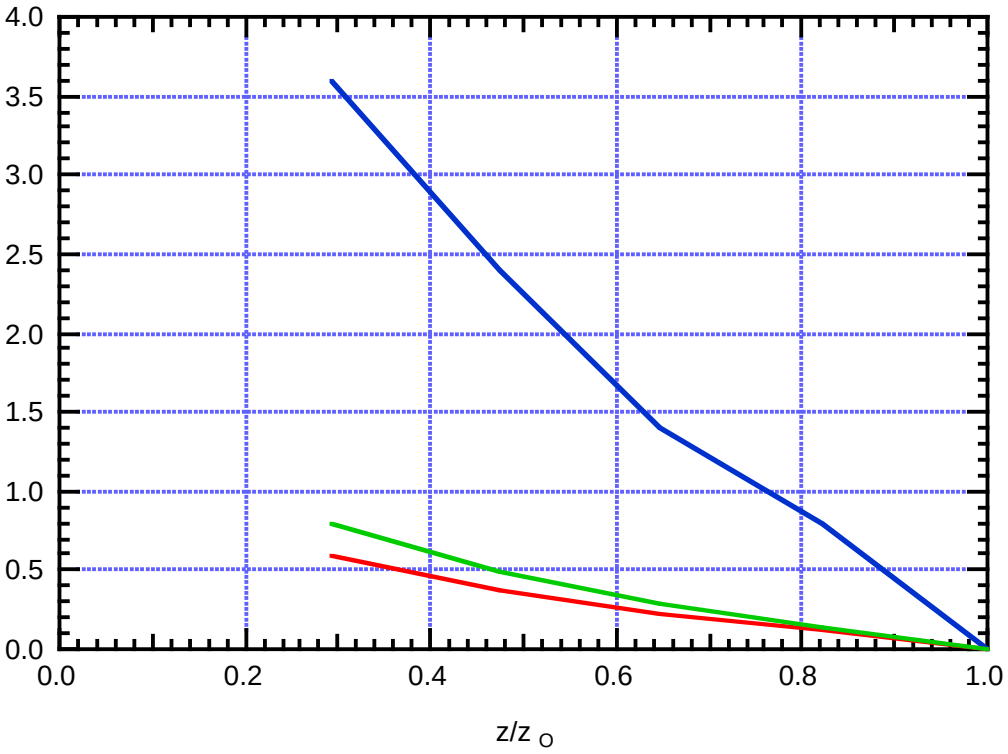

Fig. 15. Same as Fig. 12 but scale height of dust perpendicular to galactic plane is 33 pc.

We see from these figures that while the saturation b value as a function of z/z_0 varies considerably with respect to dust scale height, the saturation <A> value does not vary very much, and the saturation dispersion Δ hardly varies at all. It appears that, quite independent of dust scale height or constraints on the projected radial distance, the saturated dispersion Δ_Σ is approximately a linear function of z/z_0:

$$\Delta_S \approx 1 - \frac{z}{z_0} \qquad (32)$$

Now, the actual dispersion in the apparent magnitudes of the 42 supernovae of [Perlmutter 1999] is only about 0.25, including observational errors and uncertainties. Thus it seems clear that if our model is valid, the applicable b value must be considerably below saturation. For Model #2 with no constraint on the projected radial distance, and normal dust scale height, we obtain reasonable agreement with the date of Perlmutter 1999 when $b \approx 0.3$. This may mean that our Galaxy (or at least our local portion of the Galaxy) is somewhat dustier than the typical spiral host galaxy in the Perlmutter 1999 sample. This tentative conclusion is at once vague, hard to verify, and also hard to refute, since we are only dealing with factors of 3 or so discrepancy in dust density. However, see Sec. 6.4 which appears to support this general conclusion.

6.4 *Differential Extinction for different colors.*

In addition to <A> and Δ, the rest frame differential extinction E(B-V) is also of considerable interest. We want to calculate E(B-V) for various values of b and z/z_0 using Model #2. For this purpose, we assume that E(B-V) is related to A_B by eq. (26) with R_V given in terms of b by eq. (27). (Of course we remind ourselves that eq. (27) is just a guess). We find that $E(B-V)/A_B$ is described by the curve shown in Fig. 16. This, figure shows that the variation of $E(B-V)/A_B$ over the indicated range of b is quite modest; this suggests that the precise form of the relationship between R_V and b may not be so critical.

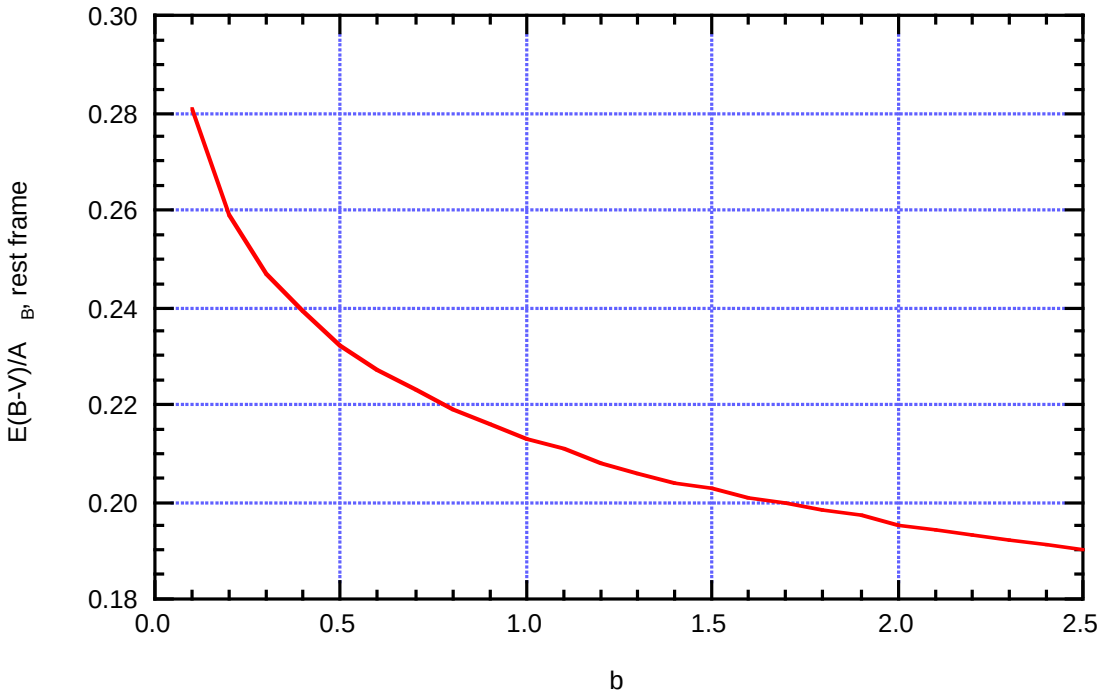

Fig. 16 Plot of $E(B-V)/A_B$ versus b assuming the validity of eq. (27).

Using Model # 2, and the values shown in Fig. 16, it is possible to calculate <E(B-V)> versus z for z_0 = .86, for various values of b, the projected radial distance from the galactic center, and the inclination angle θ. It would be interesting and worth-while to compare such calculations with existing supernova data, (for example the 42 supernovae of Perlmutter 1999}.

Finally let's consider the differential extinction for different colors in the case z_0=1.70, which might be of interest for SNAP. Here we make use of the following:

• The peak-transmission wavelengths of 10 selected filters are those chosen by Alex Kim; (see Table 2).

• The relationship between the absorption coefficient parameter b and R_V is given by eq. 27 (Table 4). This is only a crude guess, as we have already emphasized, and is almost certainly quite naïve.

•We calculate $E(\lambda_n - \lambda_m)$ for wavelengths in the rest frame by means of eq. 26, where A_B is chosen to be the average extinction as in previous figures. We then use Table 3 to give $E(\lambda_n - \lambda_m)$ in the observer frame.

Fig.17 shows the results for b=0.1. Here $E(\lambda_n - \lambda_m)$ is plotted versus the wavelength index m (in the observer frame). We can see from this plot that essentially, the dependence of $E(\lambda_n - \lambda_m)$ on m is linear; in other words, very little new knowledge is gained by looking at more than one color excess. The same conclusion results from consideration of the cases b=1, b=10 (Figs 18,19) respectively.

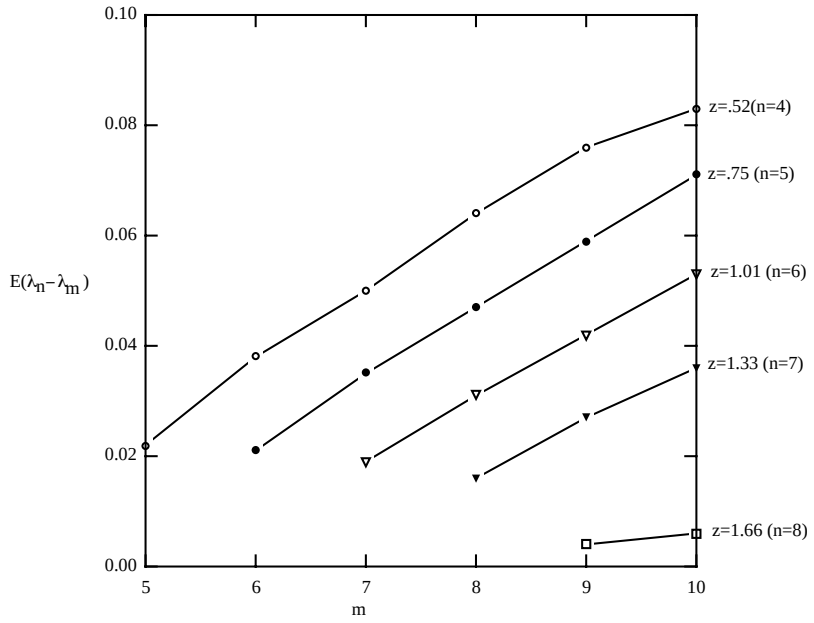

Fig. 17. $E(\lambda_n - \lambda_m)$ versus m for various red-shifts z (indices n); b=0.1.

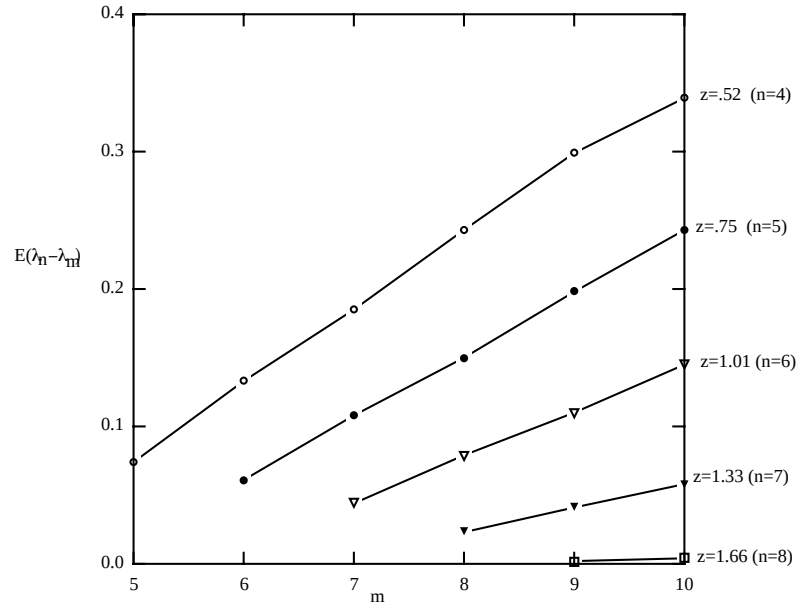

Fig. 18 b=1.0

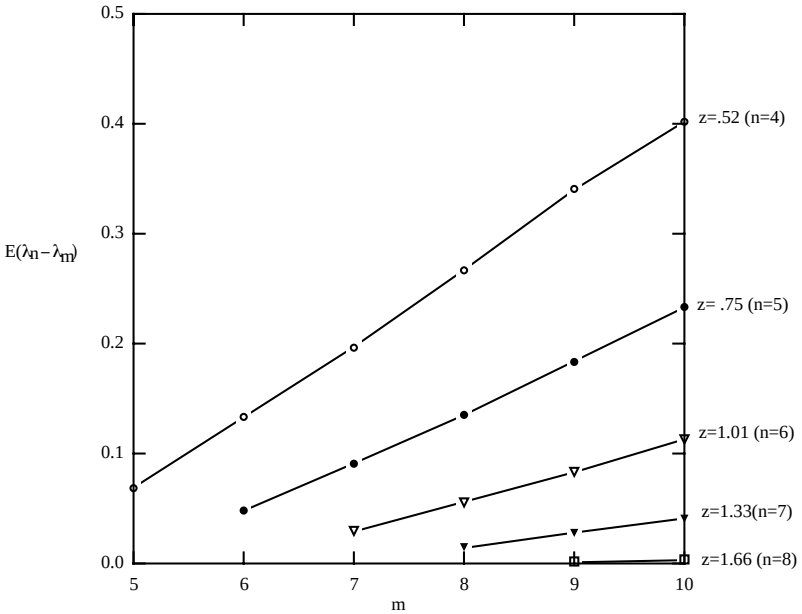

Fig. 19. b=10.

7. References

A.N. Aguirre Ap. J. **512**, L19 (1999a)
Ap. J. **525**, 583 (1999b)
• A. Aguirre and Z. Haiman Ap. J. **532**, 28 (2000)
• R. Bacon J. Appl. Phys. **31**, 283 (1960)
•J.A. Cardelli, G.C. Clayton, and J.S. Mathis Ap J.**345**, 245 (1989)
• B. Donn and G.W. Sears Nature **140**, 1208 (1963)
• B.T. Draine and H.M. Lee Ap.J. **285**, 89 (1984)
• A. Dressler "The Universe at z ≈ 1: Implications for Type 1a Supernovae" in:
"Type 1a Supernovae- Theory and Cosmology" eds J.C. Niemeyer and J.W. Truran
Cambridge Univ. Press Monograph (1999)
• E.E. Falco et al Ap. J. **523**, 617 (1999)
• E.Fitzpatrick PASP **111**, 63 (1999)
• F.C. Frank Disc. Faraday Soc. **5**, 48, 67 (1949)
• Hatano, Branch, and Deaton Ap.J. **502**, 177 (1998)
• W.C. Keel and R.E. White III Ast. J. **121** , 1442 (2001)
• C.Kittel Introduction to Solid State Physics 6th Ed. 1984 (pp 561-564)
• J.S. Mathis Ann. Rev. Astron. Astroph. **28**, 37 (1990)
• Y.C. Pei Ap.J. **395**, 130 (1992)
• S. Perlmutter et al Ap.J. **517**, 517 (1999)
• P. Predehl and S. Klose **306**, 283 (1996)
• E.E. Salpeter Ann. Rev. Astron. Astroph. **15**, 267 (1977)
• J.C. Weingartner and B.T. Draine Ap.J. **548**, 296 (2001)
• L.M. Will and P.A. Aannestad Ap.J. **526**, 242 (1999)